PHYSICAL REVIEW B **93**, 094403 (2016)

Magnon and electromagnon excitations in multiferroic $DyFeO_3$

T. N. Stanislavchuk,[1,*] Yazhong Wang,[2] Y. Janssen,[3] G. L. Carr,[4] S.-W. Cheong,[2] and A. A. Sirenko[1]

[1]*Department of Physics, New Jersey Institute of Technology, Newark, New Jersey 07102, USA*

[2]*Department of Physics and Astronomy, Rutgers Center for Emergent Materials, Rutgers University, Piscataway, New Jersey 08854, USA*

[3]*Department of Chemistry, Stony Brook University, Stony Brook, New York 11794, USA*

[4]*National Synchrotron Light Source, Brookhaven National Laboratory, Upton, New York 11973, USA*

(Received 10 November 2015; revised manuscript received 3 February 2016; published 4 March 2016)

Optical properties of orthorhombic $DyFeO_3$ single crystals have been studied in the far-infrared spectral range of 11–120 cm^{-1} at temperatures between 1.5 and 50 K and in magnetic fields up to 7 T. The temperature and magnetic-field dependencies of the antiferromagnetic (AFM) resonance spectra have been measured below and above the AFM ordering temperature of Dy^{3+} moments with $T_N^{Dy} = 4.2$ K. Hardening of the quasiferromagnetic mode frequency of the AFM resonance due to ordering of Dy^{3+} moments is observed. Below T_N^{Dy} two electric dipole-active magnetic excitations, or electromagnons, appear in the spectra at ∼20 and ∼50 cm^{-1}. The electromagnons vanish with the application of a strong magnetic field along the a or b axis which changes the magnetic structures of Fe^{3+} and Dy^{3+} moments into the ones compatible with the spatial inversion symmetry. We show that the electromagnon at ∼20 cm^{-1} provides a significant contribution to the static electric permittivity ε. The energies of the electromagnons as well as static electric permittivity manifest a strong hysteresis upon cycling of an external magnetic field at $T < T_N^{Dy}$.

DOI: 10.1103/PhysRevB.93.094403

I. INTRODUCTION

Rare-earth orthoferrites crystallize in the orthorhombically distorted perovskite structure (*Pbnm*) with four $RFeO_3$ molecules per unit cell [1]. In all studied orthoferrites the Fe-Fe exchange interaction leads to an antiferromagnetic (AFM) ordering of the Fe subsystem with a weak ferromagnetic (FM) canting due to Dzyaloshinskii-Moriya interaction at Néel temperatures T_N in the range between 650 and 700 K [2]. The resulted spin structure $\Gamma_4(G_xA_yF_z)$ persists down to the lowest temperatures in orthoferrites with nonmagnetic R ions (R = Y, La, and Lu). In other $RFeO_3$ compounds, the magnetic rare-earth ions are polarized by R-Fe exchange interaction, and the degree of polarization increases with the temperature decrease. The increase in polarization results in an increase in magnetic anisotropy of the rare-earth subsystem that can lead to a spin-reorientation (SR) transition. In most rare-earth orthoferrites, the SR transition occurs via two second-order phase transitions, which result in the change in the spin configuration of the Fe subsystem from $\Gamma_4(G_xA_yF_z)$ with the net magnetization directed along the c axis to $\Gamma_2(F_xC_yG_z)$ with the net magnetization directed along the a axis. $DyFeO_3$ is the only nonsubstituted member of the orthoferrite family in which the spin configuration of the Fe subsystem changes from weakly ferromagnetic Γ_4 to purely AFM $\Gamma_1(A_xG_yC_z)$ via the Morin-type phase transition at $T_M \sim 50$ K [3,4]. In the temperature range between 1.5 and 4 K several orthoferrites show spin ordering of the rare-earth subsystem. In particular, Dy^{3+} spins order antiferromagnetically in the $\Gamma_5(g_xa_y)$ spin configuration at $T_N^{Dy} \approx 4$ K [3,5]. Application of a high enough magnetic field along the principal crystallographic axes of $DyFeO_3$ results in SR phase transitions [4,6]. For example, application of a magnetic field along the a axis results in a spin-screw transition of the Fe subsystem from the Γ_1 configuration to the Γ_2 one, application along the b axis—in a spin-flop transition from the Γ_1 to the Γ_4 configuration and application along the c axis—in a spin-screw transition from the Γ_1 to the Γ_4 configuration.

Spin configurations Γ_1, Γ_2, and Γ_4 observed in the Fe subsystem of $DyFeO_3$ (and other rare-earth orthoferrites) are compatible with the space inversion operation and, hence, do not allow either a linear magnetoelectric (ME) effect or a spontaneous electric polarization. Below T_N^{Dy}, Dy moments order into the Γ_5 (g_xa_y) configuration which together with the Γ_1 configuration of Fe spins form a 222 nonpolar magnetic symmetry group. This symmetry still does not allow spontaneous ferroelectric polarization but, due to breaking of inversion symmetry, allows a linear magnetoelectric effect with diagonal components of the magnetoelectric tensor $\alpha_{ii}(i = x,y,z)$ [7]. A magnetic field applied along the c axis can reorient Fe spins from the Γ_1 to the Γ_4 configuration that together with the Γ_5 Dy spin configuration results in a polar magnetic group $2m'm'$ and, hence, existence of spontaneous polarization along the c axis becomes possible (the ME tensor remains diagonal so that $\alpha_{zz} \neq 0$). The appearance of spontaneous polarization along the c axis in $DyFeO_3$ below T_N^{Dy} and in high magnetic fields $H \parallel c$ (Fe spins are in the Γ_4 configuration) was reported by Tokunaga *et al.* [8]. The exchange striction between adjacent Fe^{3+} and Dy^{3+} layers was proposed as the origin of the ferroelectric polarization in the low-temperature multiferroic phase [8].

Ordering of Dy moments below T_N^{Dy} allows for a linear magnetoelectric effect and, hence, opens up a possibility for the observation of dynamic magnetoelectric effects in a form of the so-called electromagnons, which are magnetic resonances excited by the electric $\vec{e}$ vector of light [9–11]. Literature on electromagnons in magnetic oxides includes perovskite $RMnO_3$ [12–16], hexagonal $YMnO_3$ [17], RMn_2O_5 [18], $Ba_2CoGe_2O_7$ [19], and CuO [20] compounds. In iron-based multiferroics electromagnons were reported in $BiFeO_3$

*Author to whom correspondence should be addressed: stantar@njit.edu

[21,22], $SmFe_3(BO_3)_4$ [23], $Ba_2Mg_2Fe_{12}O_{22}$ [24,25], and $CuFe_{1-x}Ga_xO_2$ [26]. Although electromagnons were observed in a number of magnetoelectric materials, electromagnon spectra were not reported so far for rare-earth orthoferrites.

The spin-wave spectrum of the Fe subsystem in $DyFeO_3$ consists of four modes of homogeneous magnetic oscillations, two of which are exchange modes with frequencies $\sim$1000 cm^{-1} and the other two are acoustic modes, which at $k = 0$ correspond to quasiferromagnetic (quasi-FM) and quasiantiferromagnetic (quasi-AFM) resonances with frequencies below 20 cm^{-1}. The properties of the last two excitations were studied in literature only above the temperature of Dy-spin ordering using Raman scattering [27,28], infrared (IR) spectroscopy [29], and neutron scattering [30]. At room temperature the frequency of the quasi-AFM mode is 17 cm^{-1} and is higher than the frequency of the quasi-FM mode that is $\approx$13 cm^{-1}. With decreasing temperature, the sharp softening of the quasi-AFM mode occurs: It crosses the quasi-FM mode and reaches its minimum at the point of Morin-type SR transition at $T_M = 50$ K. At the same time, the frequency of the quasi-FM mode does not show any peculiarities at the SR phase transition. With a further decrease in the temperature, the frequency of the quasi-AFM mode increases and reaches $\approx$8 cm^{-1} at $T = 4.2$ K. The strongest anomalies at the SR phase transition were observed for the values of magnon oscillator strengths and damping constants which exhibit pronounced discontinuities [29].

Although the properties of magnetic excitations were carefully studied in literature above the temperature of Dy AFM ordering $T_N^{Dy} \approx 4$ K here we show experimental data on magnons' behavior at $T < T_N^{Dy}$ (down to 1.5 K) and in external magnetic fields up to 7 T. We also report on the observation of two electromagnons positioned at $\sim$20 and $\sim$50 cm^{-1} which appear in the spectra below T_N^{Dy}, i.e. in magnetoelectric phase of $DyFeO_3$.

II. EXPERIMENT

The floating-zone growth technique was utilized to produce bulk crystals of $DyFeO_3$. Single crystals were oriented using x-ray diffraction, cut and mechanically polished in a form of platelets oriented along the orthorhombic a, b, and c directions. The in-plane cross-sectional areas were about 5×5 mm^2, and the 0.3-mm thickness of all samples was optimized for transmission measurements. To minimize the interference fringes in optical experiments, the opposite sides of the samples were wedged at an angle of about 5°. The transmission experiments were carried out at the National Synchrotron Light Source, Brookhaven National Laboratory at the U4IR beamline equipped with a Bruker i66v IR spectrometer and a LHe-pumped ($\sim$1.6-K) bolometer. Far-IR transmittance spectra were measured using synchrotron radiation with a spectral resolution of 0.3 cm^{-1} in the spectral range between 11 and 230 cm^{-1}. The low-frequency cutoff was determined by diffraction at the entrance diamond window for the U4IR beamline. The light polarization in transmission experiments was controlled by wire-grid linear polarizers. An external magnetic field of up to 7 T was applied in the Faraday configuration so that the directions of the light propagation and the field coincided. Correspondingly, the electric and magnetic fields of light were always perpendicular to the external magnetic field. In the text below we will use the notation of transmission geometry where a subindex of the electric or magnetic fields of light will indicate its direction with respect to the crystallographic axes. For example, the e_ah_b configuration means that electric field of light $\vec{e}$ is along the a axis, magnetic field of light $\vec{h}$ is along the b axis, and the direction of light propagation and external magnetic field (if any) are both along the missing third index: the c axis. The raw data of transmittance spectra were normalized to transmittance through an empty aperture with a size equal to that of the sample. For samples with strong thickness interference fringes we normalized the transmitted intensity to that measured at high temperatures or high magnetic fields where no magnons were present. Temperature and magnetic-field dependencies for static values of $\varepsilon(H,T)$ were measured using an LCR meter at 27 kHz.

III. EXPERIMENTAL RESULTS

A. Far-IR spectra of magnons and electromagnons in a zero magnetic field

In this section we will discuss temperature and magnetic-field dependencies of transmittance spectra of $DyFeO_3$ in the far-infrared spectral range in several complementary experimental configurations e_bh_a, e_ch_a, e_bh_c, and e_ch_b. The magnon temperature dependencies and corresponding transmittance maps for the frequency-temperature parameter space are shown in Figs. 1–4 for e_bh_a, e_ch_a, e_bh_c, and e_ch_b

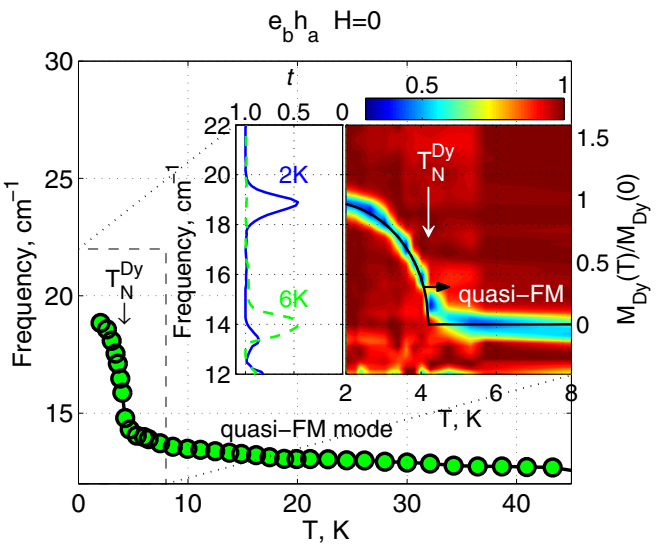

FIG. 1. Temperature dependence of the quasi-FM mode frequency (green circles) measured in $DyFeO_3$ single crystals in the e_bh_a configuration. The right part of the inset shows a normalized transmittance map vs temperature and light frequency for the temperature range around $T_N^{Dy} = 4.2$ K (the left scale is for frequency). The black curve shows temperature dependence of the relative changes in Dy magnetization $M_{Dy}(T)$ (right scale) calculated using Eq. (3). The left part of the inset shows two spectra for normalized transmittance t measured near the region of magnon absorption at 2 K ($T < T_N^{Dy}$) and 6 K ($T > T_N^{Dy}$).

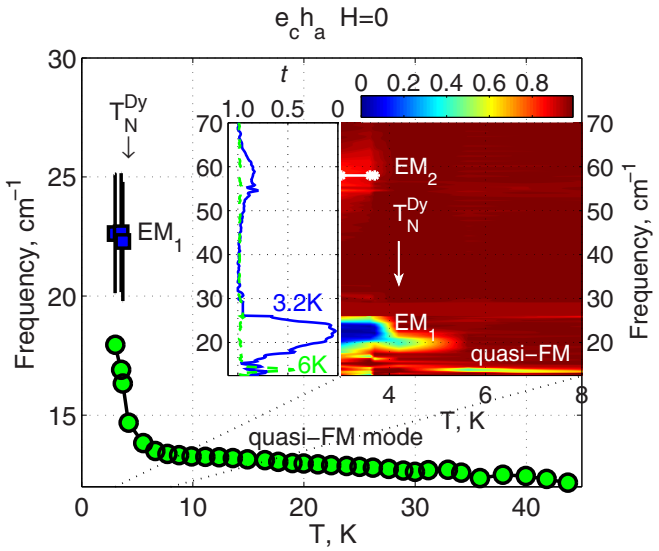

FIG. 2. Temperature dependence of the quasi-FM mode measured in the $e_c h_a$ configuration in the temperature range between 3 and 45 K. The position of two electromagnons EM_1 and EM_2 is shown with blue squares in the temperature range below $T_N^{Dy} = 4.2$ K. The right part of the inset shows a normalized transmittance map measured in the temperature range around $T_N^{Dy} = 4.2$ K. An artifact of the measurement between 27 and 29 cm^{-1}, which is due to the minimum of the beam-splitter transmittance, is smeared out in the color map. The left part of the inset shows two spectra for normalized transmittance t measured at 3.2 K ($T < T_N^{Dy}$) and 6 K ($T > T_N^{Dy}$).

configurations, respectively. To interpret the spectra of magnons we used the selection rules for magnetic dipole excitation of quasi-FM and quasi-AFM modes of AFM resonance (AFMR) in the *Pbnm* structure of $DyFeO_3$ [31,32], which are summarized in Table I. In this section we will focus first

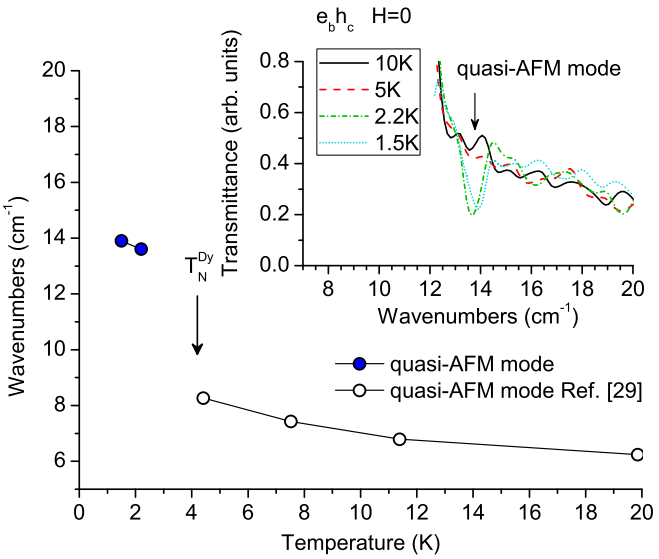

FIG. 3. Temperature dependence of the quasi-AFM mode frequency. Open circles are experimental data for the quasi-AFM mode from Ref. [29], blue circles are experimental data from this paper. The inset shows four spectra of transmittance measured at $T = 1.5$, 2.2, 5, and 10 K in the $e_b h_c$ configuration.

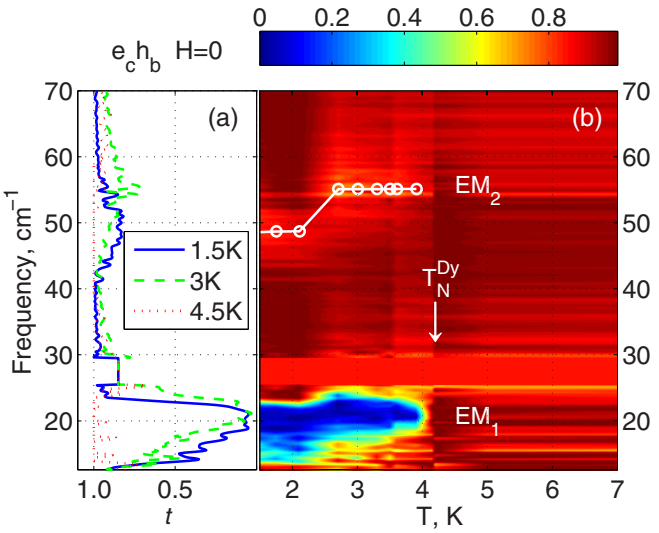

FIG. 4. Temperature dependence of normalized transmittance t measured in the $e_c h_b$ configuration in zero magnetic field ($H = 0$) near the region of EM_1 and EM_2 electromagnon absorptions. (a) Three spectra for normalized transmittance t measured at $T = 1.5$, 3, and 4.5 K. (b) A normalized transmittance map vs temperature and light frequency. An artifact of the measurement between 27 and 29 cm^{-1}, which is due to the minimum of the beam-splitter transmittance, is smeared out in the color map.

on the temperature behavior of the magnon and electromagnon modes at $H = 0$. After that we will describe the magnetic-field dependencies of the magnons and electromagnons.

1. *Quasi-FM mode*

Figure 1 shows temperature dependence of transmission spectra in the $e_b h_a$ configuration below the Morin-type phase-transition temperature $T_M \sim 50$ K when iron spins are in the $\Gamma_1(G_y)$ configuration. The experimental spectra are dominated by one absorption line positioned between 12 and 14 cm^{-1} at $T > 4.2$ K. This line is observed only in configurations with $h \parallel a$ as one can also see in the complementary $e_c h_a$ configuration (Fig. 2). We attribute it to the quasi-FM mode which, according to Table I, can be excited only by h_a component of electromagnetic field in the $\Gamma_1(G_y)$ phase. This interpretation is in agreement with Balbashov *et al.* [29] where a quasi-FM mode of AFMR positioned at 14 cm^{-1} was observed in transmission spectra of $DyFeO_3$ with $h \perp c$ at $T \geqslant 4$ K. The main new experimental finding is that at $T < 4.2$ K the frequency of the quasi-FM mode increases from

TABLE I. Selection rules for quasi-FM and quasi-AFM modes of AFMR in $DyFeO_3$ [31,32].

	Quasi-FM		Quasi-AFM	
Fe phase	Oscillation quantities	Activity	Oscillation quantities	Activity
$\Gamma_1(G_y)$	$G_z F_x$	$h \parallel a$	$G_x F_z$	$h \parallel c$
$\Gamma_2(G_z F_x)$	$F_y F_z G_x$	$h \parallel b, h \parallel c$	$G_y F_x G_z$	$h \parallel a$
$\Gamma_4(G_x F_z)$	$G_z F_x F_y$	$h \parallel a, h \parallel b$	$G_y G_x F_z$	$h \parallel c$

14 to 19 cm^{-1}. This magnon hardening at low temperatures can be naturally attributed to the magnetic ordering of Dy spins in the ab plane.

2. *Quasi-AFM mode*

Figure 3 shows temperature dependence of transmission spectra in the $e_b h_c$ configuration for the temperature range between 1.5 and 10 K. Below $T_N^{Dy} = 4.2$ K, a narrow absorption line is observed at $\approx$14 cm^{-1}. This line is observed only in $h \parallel c$ configurations at $T < T_N^{Dy}$. For example it is also observed in the magnetic-field dependence of transmission spectra in the $e_a h_c$ configuration at $H = 0$ and $T = 1.5$ K (see Fig. 5). Thus we attribute this line to a purely magnetic dipole polarized along the c axis. We note here that this magnon mode is clearly distinguished from the quasi-FM one as the latter has energy of about 19 cm^{-1} at $T = 1.5$ K (see Fig. 1). We assume that the excitation we observe in Figs. 3 and 5 is a quasi-AFM mode. Indeed, in the $\Gamma_1(G_y)$ phase of Fe spins the quasi-AFM mode can be excited by the h_c component of the electromagnetic field only (see Table I). Balbashov *et al.* [29] reported the observation of the quasi-AFM mode in $h \parallel c$ polarized transmission spectra of $DyFeO_3$. At $T = 4.2$ K the quasi-AFM mode's energy is 8 cm^{-1} that is beyond our accessible spectral range and thus we cannot observe it in our spectra. But as the temperature goes below $T_N^{Dy} = 4.2$ K, the AFM ordering of Dy spins enhances the energy of the quasi-AFM mode from 8 cm^{-1} at $T = 4.2$ K to 14 cm^{-1} at $T = 1.5$ K that is now falling into the accessible spectral range for our measurements. The increase in the quasi-AFM mode energy by 6 cm^{-1} is quite reasonable taking into account that magnetic ordering of Dy spins increases the energy of the quasi-FM mode by 5 cm^{-1}, namely, from 14 cm^{-1} at 4.2 K to 19 cm^{-1} at 1.5 K as shown in Fig. 1.

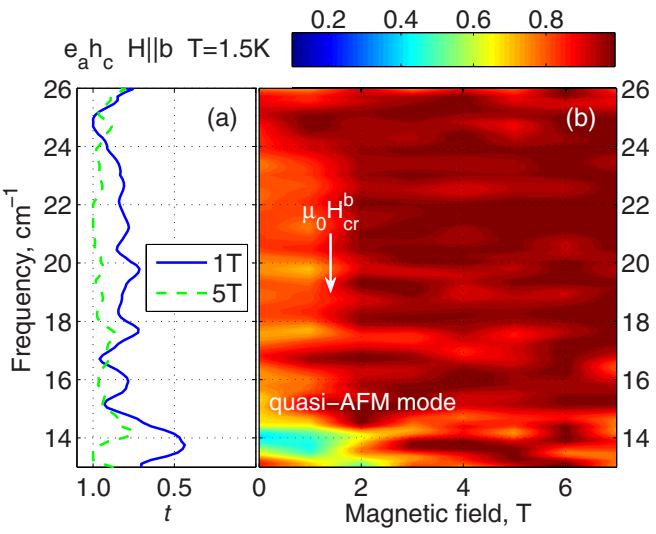

FIG. 5. Magnetic-field ($H \parallel b$) dependence of normalized transmittance t measured in the $e_a h_c$ configuration at $T = 1.5$ K. (a) Two spectra for normalized transmittance t measured at $\mu_0 H =$ 1 T($H < H_{cr}^b$) and 5 T($H > H_{cr}^b$). (b) A normalized transmittance map vs magnetic field and light frequency. The quasi-AFM mode is field independent below $\mu_0 H_{cr}^b = 1.3$ T.

B. Electromagnon excitations

Figure 2 shows that in the $e_c h_a$ configuration two wide absorption lines appear below T_N^{Dy}: a strong one at 22 cm^{-1} denoted EM_1 and a weaker one at 58 cm^{-1} denoted EM_2. These lines are observed only in the $e \parallel c$ configurations and only below T_N^{Dy}. For example, they are also seen in the $e_c h_b$ configuration at $T < 4.2$ K (see Fig. 4) but cannot be detected in the orthogonal $e_b h_a$ configuration (Fig. 1). Thus, EM_1 and EM_2 lines are electric dipole active along the c axis. Among the possible candidates for electric dipole excitations in the far-IR spectral region are phonons and crystal-field (CF) transitions in Dy^{3+} ions. The lowest-frequency phonon in rare-earth orthoferrites is known to be at $\sim$100 cm^{-1} [28], which is well above the frequency of the observed two lines. Now let us discuss whether electronic transitions in Dy^{3+} ions can be responsible for EM_1 and EM_2 lines. The Dy ions occupy four sites in the crystalline unit cell of the $DyFeO_3$ orthoferrite and have two nonequivalent positions described by the point symmetry group C_s. Since Dy^{3+} is a Kramer's ion, i.e., has odd number of electrons, the local CF of C_s symmetry splits the multiplets of the Dy^{3+} ions into Kramer's doublets, which remain doubly degenerate at the absence of a magnetic field (external or internal due to magnetic ordering). Thus, the ground multiplet $^6H_{15/2}$ of the Dy^{3+} ions is split into eight doublets by the CF of $DyFeO_3$. The early spectroscopic study of $DyFeO_3$ in the IR spectral region by Schuchert *et al.* in 1960s [33] showed that the first four CF doublets of the Dy^{3+} ions are at 0, 52, 147, and 225 cm^{-1} correspondingly. Although the Dy^{3+} doublet at 52 cm^{-1} is somewhat close to the observed EM_2 line at 58 cm^{-1}, the EM_1 line at 22 cm^{-1} does not correlate with the Dy^{3+} CF spectrum. Furthermore, magnetization [3] and Mössbauer [34] measurements of $DyFeO_3$ have shown that the ground doublet of the Dy^{3+} ions can be interpreted as a close to a pure $|\pm 15/2\rangle$ state with the axis of quantization lying in the ab plane at an angle of $\varphi_0 \approx \pm 60^\circ$ to the a axis (the signs $\pm$ in the value of φ_0 correspond to two nonequivalent positions of Dy ions). As a result, the g-factor tensor of the ground Dy^{3+} doublet is highly anisotropic: $g_{z'} \approx 19.7$, $g_{x'} = g_{y'} = 0$ (in the $x'y'z'$ coordinate system, z' is directed along the axis of quantization, and x' is directed along the c axis). Such a big value of $g_{z'}$ should result in splitting of the ground doublet in the external magnetic field applied along (or having projection on) the axis of quantization z' and thus in shifting of the CF lines corresponding to the transitions from the ground doublet to the excited doublets of the Dy^{3+} ions. As we will show in the next section, the application of the external magnetic field along the a and b crystallographic axes has not led to any noticeable shift of the EM_1 and EM_2 lines (see Figs. 9 and 11) pointing that they are not related to the CF transitions. Moreover, although the ground doublet of Dy^{3+} does not have a nonzero g factor along the c axis, the Dy subsystem does possess an appreciable magnetic susceptibility χ_c along the c axis at low temperatures [35]. It was shown [36] that χ_c can be explained by Van Vleck contribution from the first excited CF level of Dy^{3+} ions, and the calculated value of χ_c is in good agreement with the magnetization measurements [35] provided that the first excited CF level is at $\sim$52 cm^{-1}. Finally Mössbauer measurements [34] of $DyFeO_3$ at temperatures up

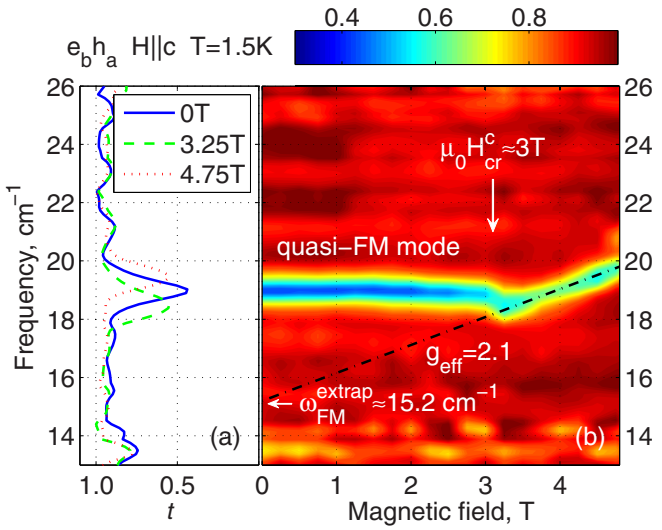

FIG. 6. Magnetic-field ($H \parallel c$) dependence of normalized transmittance t measured in the $e_b h_a$ configuration at $T = 1.5$ K. (a) Three spectra for normalized transmittance t measured at $\mu_0 H = 0\,\mathrm{T}(H<H^c_{cr})$, 3.25 T, and 4.75 T ($H>H^c_{cr}$). (b) A normalized transmittance map vs magnetic field and light frequency. The dashed straight line shows linear dependence of the quasi-FM mode on the field for $H>H^c_{cr}$ with an effective g-factor of 2.1.

to 50 K are consistent with population of only the ground Dy doublet, thus proving that the first excited CF level is above 50 K ($\sim$35 cm^{-1}). Based on the above arguments, we can exclude both phonons and electronic transitions from the candidates of excitations responsible for the observed EM_1 and EM_2 absorption lines. We note, that EM_1 and EM_2 lines appear only below T_N^{Dy} when linear magnetoelectric effect is allowed. As we will show in the next section, the application of strong enough magnetic field along the a or b axis, which changes the magnetic structures of Fe^{3+} and Dy^{3+} moments into the ones compatible with spatial inversion symmetry, results in vanishing of the EM_1 and EM_2 lines (see Figs. 9 and 11). Thus we conclude that these lines are observed only in the magnetoelectric phase of $DyFeO_3$ and attribute them to electric dipole active magnetic excitations or electromagnons.

C. Far-IR spectra of magnons and electromagnons in an external magnetic field

1. *Quasi-FM mode*

As was shown above, in the $\Gamma_1(G_y)$ state of Fe spins the quasi-FM mode is polarized along the a axis ($h||a$) and thus is observed in transmission spectra in two complementary configurations: $e_b h_a$ and $e_c h_a$. It is convenient to choose the $e_b h_a$ configuration to monitor the behavior of the quasi-FM mode since in this configuration the quasi-FM mode is not overlapped with EM_1 absorption which is observed in the $e_c h_a$ configuration below T_N^{Dy} (see Fig. 2). Figure 6 shows magnetic-field dependence ($H \parallel c$) of the quasi-FM mode measured in the $e_b h_a$ configuration at $T = 1.5$ K. At $H = 0$ the Fe subsystem is in the $\Gamma_1(G_y)$ state and the Dy subsystem is in the $\Gamma_5(g_x a_y)$ state. With the field increase the magnon's frequency is insensitive to magnetic fields up to $\mu_0 H^c_{cr} \approx 3$ T. At H^c_{cr} the Fe subsystem reorients from the $\Gamma_1(G_y)$ state to the canted $\Gamma_4(G_x F_z)$ state while the magnetic structure of the Dy moments remains unchanged. At $H>H^c_{cr}$ quasi-FM mode frequency ω_{FM} reveals a close to linear dependence on H with the effective g-factor $g_{eff} \approx 2.1$ which we define as follows: $\Delta\omega_{FM} = g_{eff}\mu_B\mu_0\Delta H$, where $\Delta\omega_{FM}$ is a frequency shift measured in (cm^{-1}) induced by a change in the magnitude of the magnetic field by ΔH, μ_B is a Bohr magneton ($\mu_B \approx 0.4669\,\mathrm{cm}^{-1}\,\mathrm{T}^{-1}$), and μ_0 is a magnetic constant. The extrapolated value of ω_{FM} at $H>H^c_{cr}$ towards $H = 0$ is $\omega^{extrap}_{FM} \approx 15.2\,\mathrm{cm}^{-1}$ which is close to the frequency of

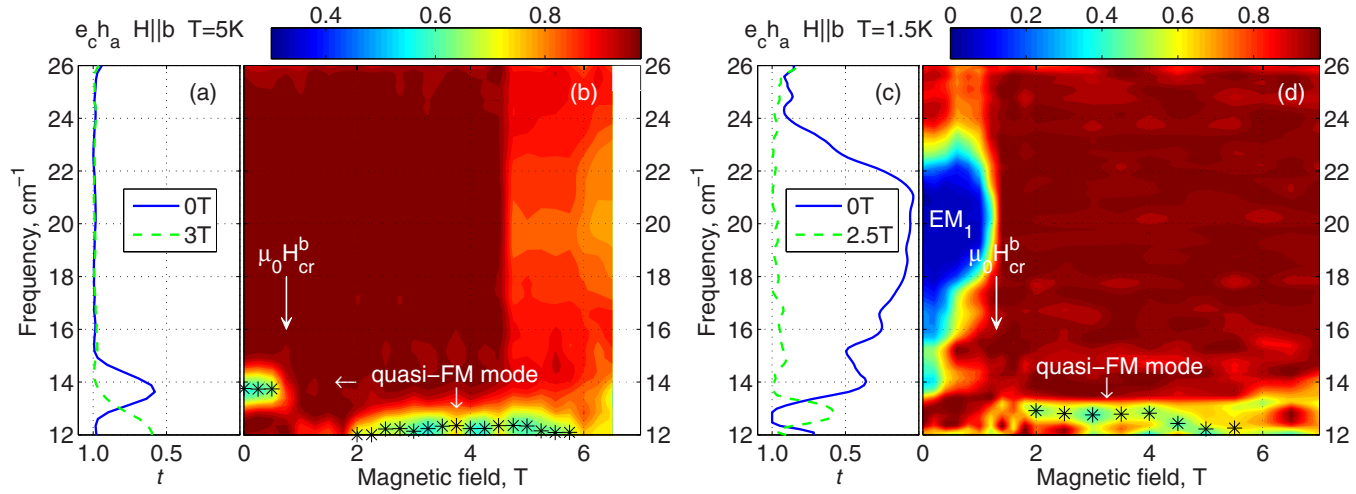

FIG. 7. Magnetic-field ($H \parallel b$) dependence of normalized transmittance t measured in the $e_c h_a$ configuration at (a) and (b) $T = 5$ K and (c) and (d) 1.5 K. (a) Two spectra for normalized transmittance t measured at $\mu_0 H = 0\,\mathrm{T}(H<H^b_{cr})$ and 3T ($H>H^b_{cr}$). (b) A normalized transmittance map vs magnetic field ($H \parallel b$) and light frequency measured at $T = 5$ K. (c) Two spectra for normalized transmittance t measured at $\mu_0 H = 0\,\mathrm{T}(H<H^b_{cr})$ and 2.5 T ($H>H^b_{cr}$). (d) A normalized transmittance map vs magnetic field ($H \parallel b$) and light frequency measured at $T = 1.5$ K. Critical magnetic fields $\mu_0 H^b_{cr}$ of 0.6 T at $T = 5$ K and 1.3 T at $T = 1.5$ K are shown in (b) and (d) with vertical arrows. Stars in (b) and (d) show the positions of the quasi-FM modes.

the quasi-FM mode $\omega_{\rm FM}|_{T=5K}^{H=0} \approx 14\,{\rm cm}^{-1}$ in zero field and temperatures just above $T_N^{\rm Dy}$ (see Fig. 1) when Fe spins are in $\Gamma_4(G_xF_z)$ phase and Dy ions are paramagnetic.

Figure 7 shows magnetic-field dependence ($H \parallel b$) of transmittance measured in the e_ch_a configuration at $T = 5\,{\rm K}$ (a) and (b) and at $T = 1.5\,{\rm K}$ (c) and (d). At $T = 5\,{\rm K}$ and $H = 0$ the quasi-FM mode is observed at $13.7\,{\rm cm}^{-1}$. With the field increase above $\mu_0 H_{cr}^b \approx 0.6\,{\rm T}$, the quasi-FM mode vanishes but above 2 T another magnon is observed at $\sim 12.5\,{\rm cm}^{-1}$, and its position practically does not change with the further increase in magnetic field. The magnetic field applied along the b axis causes the SR transition of the Fe subsystem from $\Gamma_1(G_y)$ to $\Gamma_4(G_xF_z)$ spin configuration [6]. Thus the magnon at $\sim 12.5\,{\rm cm}^{-1}$ is observed in the $\Gamma_4(G_xF_z)$ phase of Fe spins ($H > H_{cr}^b$) and is magnetic dipole active along the a axis (the e_ch_a configuration of measurements). Based on selection rules from Table I, we attribute this magnon to the quasi-FM mode, which is active in the $\Gamma_4(G_xF_z)$ phase for $h \parallel a$.

At $T = 1.5\,{\rm K}$ and $H = 0$ [Figs. 7(c) and 7(d)] the quasi-FM mode, enhanced by Dy ordering, is at $\sim 19\,{\rm cm}^{-1}$ (see, for example, Fig. 1) that falls into the region of EM_1 absorption and is not explicitly observed in our spectra. Above $\mu_0 H_{cr}^b \approx 1.3\,{\rm T}$ the EM_1 and quasi-FM mode absorptions vanish due to the onset of a $\Gamma_1 \rightarrow \Gamma_4$ spin-reorientation transition of Fe spins accompanied by the reorientation of Dy moments from the $\Gamma_5(g_xa_y)$ to the Γ_3 (f_yc_x) state [37]. At $\mu_0 H_b > 2\,{\rm T}$, the quasi-FM mode appears at $\sim 12.5\,{\rm cm}^{-1}$ [Figs. 7(c) and 7(d)] just like in the case of spectra at $T = 5\,{\rm K}$ [Figs. 7(a) and 7(b)]. We note that the frequency of the quasi-FM mode in the field-induced Γ_4 state of Fe spins and extrapolated towards $H = 0$ is different for $H \parallel c$ [$\omega_{\rm FM}^{\rm extrap} \approx 15.2\,{\rm cm}^{-1}$; see Fig. 6(b)] and for $H \parallel b$ [$\omega_{\rm FM} \approx 12.5\,{\rm cm}^{-1}$; see Figs. 7(b) and 7(d)]. The difference can be due to different magnetic structures of the Dy subsystem. For $H||b$ and $T = 1.5\,{\rm K}$ the Dy structure is Γ_3 (f_yc_x) above $\mu_0 H_b \approx 2\,{\rm T}$, where $\omega_{\rm FM} \approx 12.5\,{\rm cm}^{-1}$ is observed. For $H \parallel b$ and $T = 5\,{\rm K}$ the Dy subsystem is paramagnetic and is polarized by the external magnetic field in the Γ_3 (f_yc_x) configuration. At $\mu_0 H_b \approx 2\,{\rm T}$ the splitting of the ground Dy doublet is $\Delta = g_{z'}\mu_B\mu_0 H_b \sin\varphi_0 \approx 14.5\,{\rm cm}^{-1}(\approx 20\,{\rm K})$. Such a splitting at $T = 5\,{\rm K}$ means that only the lowest sublevel of the split ground Dy doublet is populated and the magnetization of Dy is close to saturation. Thus the magnetic state of the Dy moments at $\mu_0 H_b > 2\,{\rm T}$ is approximately the same for both $T = 5$ and $T = 1.5\,{\rm K}$, which results in the same frequency $\omega_{\rm FM} \approx 12.5\,{\rm cm}^{-1}$ of the quasi-FM mode. In contrast to the case of $H \parallel b$, for $H \parallel c$ and $T = 1.5\,{\rm K}$ the magnetic structure of the Dy spins is $\Gamma_5(g_xa_y)$ and does not change with the field increase. The $\Gamma_5(g_xa_y)$ structure of the Dy spins renormalizes the frequency of the quasi-FM mode in a different way than the Γ_3 (f_yc_x) structure does, which results in the observed difference between $\omega_{\rm FM}^{\rm extrap} \approx 15.2\,{\rm cm}^{-1}$ at $H \parallel c$ [see Fig. 6(b)] and $\omega_{\rm FM} \approx 12.5\,{\rm cm}^{-1}$ at $H \parallel b$ [see Figs. 7(b) and 7(d)].

2. *Quasi-AFM mode*

In the $\Gamma_1(G_y)$ state of Fe spins the quasi-AFM mode is polarized along the c axis ($h \parallel c$) and thus is observed in the e_ah_c and e_bh_c configurations. Figure 8 shows a magnetic-field dependence ($H \parallel a$) of transmittance measured in the e_bh_c

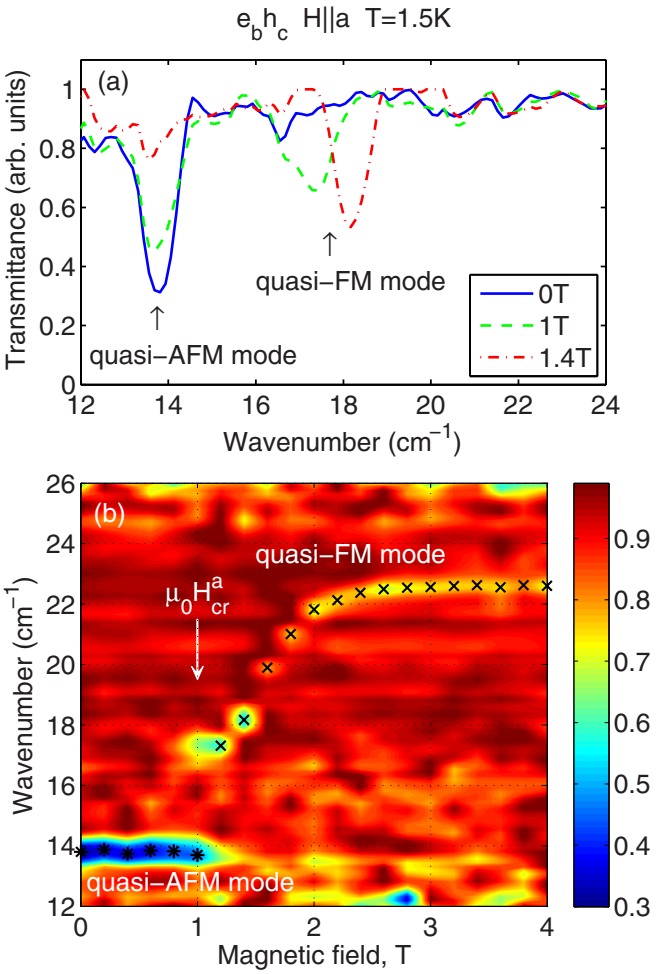

FIG. 8. Magnetic-field ($H \parallel a$) dependence of normalized transmittance t measured in the e_bh_c configuration at $T = 1.5\,{\rm K}$. (a) Three spectra for normalized transmittance t measured in the interval of magnetic fields around SR transition at about $\mu_0 H_{cr}^a = 1\,{\rm T}$. Two AFMR modes are observed simultaneously at $H = H_{cr}^a$. (b) A normalized transmittance map vs magnetic field ($H \parallel a$) and light frequency. The positions of quasi-FM and quasi-AFM modes are marked with crosses and stars correspondingly.

configuration at $T = 1.5\,{\rm K}$. The quasi-AFM mode is observed at $\omega_{\rm AFM} \approx 14\,{\rm cm}^{-1}$ for $H = 0$, and its frequency is insensitive to magnetic fields up to $\mu_0 H_{cr}^a = 1\,{\rm T}$. Just above H_{cr}^a, another line appears at $\sim 17\,{\rm cm}^{-1}$, and its frequency gradually increases and stabilizes at $22.5\,{\rm cm}^{-1}$ in the field of 2 T. The magnetic field applied along the a axis causes a spin-screw transition of the Fe subsystem from the $\Gamma_1(G_y)$ to the $\Gamma_2(G_zF_x)$ configurations [4,6] accompanied by spin reorientation of Dy moments from the $\Gamma_5(a_yg_x)$ to the Γ_2 (f_xc_y) state. According to selection rules from Table I, in the $\Gamma_2(G_zF_x)$ phase of Fe spins the quasi-AFM mode can be excited by the h_a component of the electromagnetic field only and thus cannot be observed in the e_bh_c configuration in Figs. 8(a) and 8(b) for $H > H_{cr}^a$. Instead, in the $\Gamma_2(G_zF_x)$ phase the conditions for the excitation of the quasi-FM mode are $h \parallel b$ or $h \parallel c$. Thus we concluded that the line observed in Figs. 8(a) and 8(b) for $H > H_{cr}^a$ is the quasi-FM mode. The fact that its frequency gradually increases and stabilizes at $22.5\,{\rm cm}^{-1}$ in the field of 2 T might

indicate that between 1 and 2 T Fe spins continue to rotate from the Γ_1 structure to the Γ_2 structure until they stabilize at 2 T. Indeed, as was shown by Gnatchenko *et al.* [38] the reorientation of the Fe spins in $H \parallel a$ at $T < T_M$ ($T_M \sim 50$ K is a temperature of Morin transition) occurs in a sequence $\Gamma_4\ (G_y) \rightarrow \Gamma_{12}(F_xG_yG_z) \rightarrow \Gamma_2(F_xG_z)$ through continuous rotation of G vector and is completed by a second-order phase transition to a Γ_2 phase. The stabilization of the quasi-FM mode's frequency above 2 T indicates that the mode's effective g-factor along the a axis when Fe spins are in the Γ_2 phase is negligible in the studied magnetic-field region (up to 4 T).

The magnetic-field dependence of transmittance ($H \parallel b$) in the e_ah_c configuration at $T = 1.5$ K is shown in Fig. 5. The quasi-AFM mode is observed at 14 cm^{-1} at zero magnetic field, and its frequency is insensitive to magnetic fields up to $\mu_0 H^b_{cr} \approx 1.3$ T. At $H > H^b_{cr}$ the quasi-AFM mode absorption vanishes. It was shown [4,6] that a magnetic field applied along the b axis of $DyFeO_3$ causes spin reorientation of the Fe subsystem from the $\Gamma_1(G_y)$ to the $\Gamma_4(G_xF_z)$ state accompanied by the reorientation of Dy moments from the $\Gamma_5(a_yg_x)$ to the $\Gamma_3\ (f_yc_x)$ state [37]. In the field-induced Γ_4 phase of Fe spins the quasi-AFM mode is excited by the h_c component of the electromagnetic field, just like in the $\Gamma_1(G_y)$ phase (see Table I). Thus the quasi-AFM mode is expected to be observed in e_ah_c spectra for both $H < H^b_{cr}(\Gamma_1$ state) and $H > H^b_{cr}(\Gamma_4$ state) whereas in our measurements it was observed only for $H < H^b_{cr}$ (see Fig. 5). As was shown above, the ordering of the Dy subsystem in the $\Gamma_5(a_yg_x)$ state increases the quasi-FM mode's frequency from 14 to 19 cm^{-1} (see Fig. 1) when the Fe subsystem is in the Γ_1 configuration whereas the field-induced ($H \parallel b$) reorientation of Fe spins from the $\Gamma_1(G_y)$ to the $\Gamma_4(G_xF_z)$ state accompanied by the reorientation of Dy moments from the $\Gamma_5(a_yg_x)$ to the $\Gamma_3\ (f_yc_x)$ state decreases the quasi-FM mode's frequency from 19 cm^{-1} (see Fig. 1) down to $\sim$12.5 cm^{-1} [see Fig. 7(d)]. Previously we concluded that the observation of the quasi-AFM mode at $T = 1.5$ K is possible because Dy ordering in $\Gamma_5(a_yg_x)$ state increases the quasi-AFM mode's frequency from 8 to 14 cm^{-1}. Hence, we assume that at $H > H^b_{cr}$ when the Fe and Dy subsystems are reoriented into $\Gamma_4(G_xF_z)$ and $\Gamma_3\ (f_yc_x)$ configurations correspondingly, the frequency of the quasi-AFM mode is decreased, just like in the case of ω_{FM}, so that it no longer falls into the spectral region of our measurements.

3. *Electromagnons*

Transmission spectra of a $DyFeO_3$ crystal at zero magnetic field revealed two EM_1 and EM_2 absorption lines at 22 cm^{-1} and 58 cm^{-1} which appear at $T < T_N^{Dy}$ and are electric dipole active along the c axis. Figure 9(b) shows a magnetic-field dependence ($H \parallel b$) of transmission spectra in the e_ch_a configuration at $T = 1.5$ K in the region from 0 to 2 T. At $H = 0$ the EM_1 and EM_2 lines are at 20 and 50 cm^{-1} correspondingly. With the increase in magnetic field, the $EM_{1,2}$ lines become weaker and vanish at $\mu_0 H^b_{cr} \approx 1.3$ T when the spin reorientations of the Fe spins from the $\Gamma_1(G_y)$ to the $\Gamma_4(G_xF_z)$ state and Dy moments from the $\Gamma_5(a_yg_x)$ to the $\Gamma_3\ (f_yc_x)$ state occur. In contrast to the $\Gamma_5(g_xa_y)$ configuration, the $\Gamma_3\ (f_yc_x)$ configuration of Dy moments is compatible with spatial inversion symmetry [7] and thus at $H > H^b_{cr}$, when $EM_{1,2}$ absorptions vanish, the magnetoelectric effect in $DyFeO_3$ is not allowed. Similar behavior of $EM_{1,2}$ lines is observed in transmission spectra when the magnetic field is directed along the a axis. Figure 11(b) shows a magnetic-field dependence ($H \parallel a$) of transmission spectra in the e_ch_b configuration at $T = 1.5$ K in the region from 0 to 3 T. At $H = 0$ the EM_1 and EM_2 lines are at 18 and 48 cm^{-1} correspondingly. At $H^a_{cr} \approx 1$ T the reorientation transition of Fe spins from the $\Gamma_1(G_y)$ to the $\Gamma_2(F_xG_z)$ state and Dy moments from the $\Gamma_5(g_xa_y)$ to the $\Gamma_2\ (f_xc_y)$ state occur and $EM_{1,2}$ absorptions vanish. Just as in the case of the $\Gamma_3\ (f_yc_x)$ configuration, the $\Gamma_2\ (f_xc_y)$ configuration of Dy moments is compatible with spatial inversion, and, hence, magnetoelectricity is not allowed [7]. Since EM_1 and EM_2 absorptions are observed only in magnetoelectric phases of $DyFeO_3$ and, as was shown above, are not related to phonon modes or electronic transitions in Dy^{3+} ions, we attribute them to electric dipole-active magnetic excitations or electromagnons. The existence of electric dipole-active magnetic excitations in rare-earth orthoferrites was theoretically predicted by Yablonskii and Krivoruchko back in 1988 [39] and attributed to rare-earth magnetic modes which are odd under inversion symmetry. Our experimental observation of electromagnons in $DyFeO_3$ at the temperatures below the magnetic ordering of Dy^{3+} moments is in agreement with that theoretical prediction. The exact mechanisms of such dynamic excitations that definitely include ordered rare-earth spins would require a separate theoretical study. The role of Fe^{3+} spins may not be strong because both the EM_1 electromagnon and the quasi-FM mode were observed simultaneously in Figs. 2 and 9(c). Note, however, that the appearance of EM_1 correlated with a decrease of the oscillator strength for quasi-FM mode at low temperatures compared to that at $T > 4$ K (see inset in Fig. 2) thus indicating a possible contribution of Fe^{3+} spins into the formation of electromagnon excitations.

The EM_1 and EM_2 electromagnons demonstrate strong hysteresis upon cycling of an external magnetic field along the b axis [see Figs. 9(a)–9(d)]. At $H = 0$ the EM_1 and EM_2 lines are at 20 and 50 cm^{-1} correspondingly. With the increase in magnetic field along the b axis, the $EM_{1,2}$ lines become weaker and vanish at $\mu_0 H^b_{cr} \approx 1.3$ T. Upon decreasing the magnetic field below H^b_{cr} only one broad electromagnon EM_1 is observed at 30 cm^{-1}. With further decreasing the magnetic field another phase transition takes place at $\mu_0 H^b_{cr2} \approx 0.2$ T, and the EM_1 at 30 cm^{-1} vanishes whereas the EM_1 at $\sim$20 cm^{-1} appears again as at zero field. The weak EM_2 electromagnon at 50 cm^{-1} was not "restored" (at least it is not clearly seen in our spectra) even when we reduced the magnetic field to zero. The observation of EM_1 electromagnon at 30 cm^{-1} can indicate on the existence of an intermediate state of Fe/Dy magnetic moments upon sweeping the magnetic field down at $T < T_N^{Dy}$ when spin reorientation of Fe subsystem from the Γ_4 to the Γ_1 configuration takes place. As was shown by Gnatchenko *et al.* [37] the spin reorientation in $DyFeO_3$ in $H \parallel b$ and $T < T_N^{Dy}$ can occur in two stages: $\Gamma_1\ (G_y) \rightarrow \Gamma_{1234}(F_xF_yF_zG_xG_yG_z) \rightarrow \Gamma_4(F_xG_y)$ for Fe spins and $\Gamma_5\ (g_xa_y) \rightarrow \Gamma_{2358}(g_{xy}a_{xy}f_{xy}c_{xy}) \rightarrow \Gamma_3(f_yc_x)$ for Dy spins. The observation of EM_1 at 30 cm^{-1} may be related to irreversibility of the above sequence of phases in

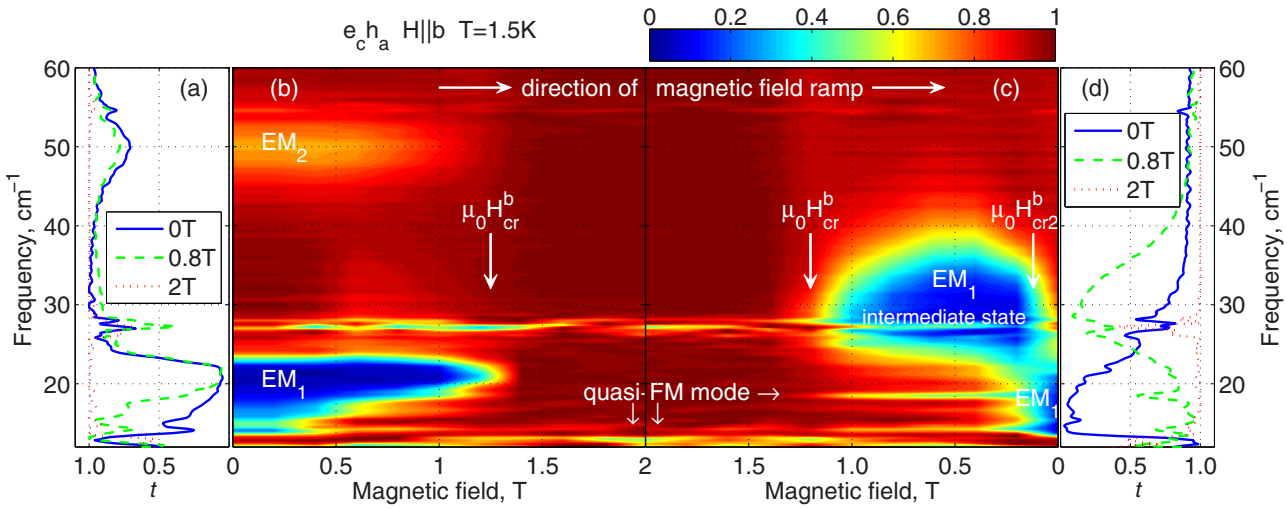

FIG. 9. Magnetic-field ($H \parallel b$) dependence of normalized transmittance t measured in the $e_c h_a$ configuration at $T = 1.5$ K during ramping field (a) and (b) up and (c) and (d) down. (a) Three spectra for normalized transmittance t measured during ramping field up for $\mu_0 H =$ 0 T, 0.8 T ($H < H^b_{cr}$) and 2 T ($H > H^b_{cr}$). (b) A normalized transmittance map vs magnetic field and light frequency measured during ramping field up. (c) A normalized transmittance map measured during ramping field down. (d) Three spectra for normalized transmittance t measured at $\mu_0 H = 0$ T ($H < H^b_{cr2}$), 0.8 T($H^b_{cr2} < H < H^b_{cr}$), and 2 T ($H > H^b_{cr}$) during ramping field down. A quasi-FM mode is marked with a white arrow. Critical magnetic fields $\mu_0 H^b_{cr} \approx 1.3$ T in (b) and (c) and $\mu_0 H^b_{cr2} \approx 0.2$ T in (c) are shown with vertical arrows. An artifact of the measurement between 27 and 29 cm^{-1} is due to the minimum of the beam-splitter transmittance.

Fe and Dy subsystems upon sweeping of the magnetic field. Also we note that an irreversible state of Fe spins was recently observed in $DyFeO_3$ at $T < T_N^{Dy}$ upon sweeping the magnetic field along the c axis [40].

The existence of an EM_1 electromagnon with a strong frequency hysteresis upon cycling of the magnetic field should result in a hysteresis in the corresponding component of the static dielectric constant $\varepsilon(H)$. Figure 10(a) shows the $\varepsilon_c(H)$ hysteresis loop measured at 2 K in magnetic fields $H \parallel b$ and electric field $E \parallel c$, the latter having a sweep frequency of $f = 27$ kHz. As the field is ramped up from 0 to 2 T, $\varepsilon_c(H)$ drastically drops from 24.2 to 23.1 at $\mu_0 H^b_{cr} = 0.4$ T when the Fe subsystem reorients from the Γ_1 to the Γ_4 spin configuration. As the field is ramped down, the quasistatic ε partially restores at $\mu_0 H^b_{cr} = 0.4$ T and then, as the field is further removed from 0.4 T to 0, it gradually restores to the initial value of 24.1. Thus, both the EM_1 electromagnon and the static ε demonstrate hysteresis upon cycling of the magnetic field at $T < T_N^{Dy}$. We note here that the value of the critical magnetic fields H^b_{cr} at which the spin-flop transition of the Fe subsystem takes place is different in the IR transmittance ($\mu_0 H^b_{cr} \approx 1.3$ T) and dielectric ($\mu_0 H^b_{cr} = 0.4$ T) measurements. As was shown in Ref. [37] the value of H^b_{cr} is sensitive to the angle β between the direction of the magnetic field and the b axis of the crystal. Thus the observed difference in H^b_{cr} might be related to slightly different angles β in optical and dielectric measurements.

Figure 11 shows magnetic-field dependence ($H \parallel a$) of transmission spectra measured in the $e_c h_b$ configuration at $T = 1.5$ K during cycling magnetic field up (a) and (b) and

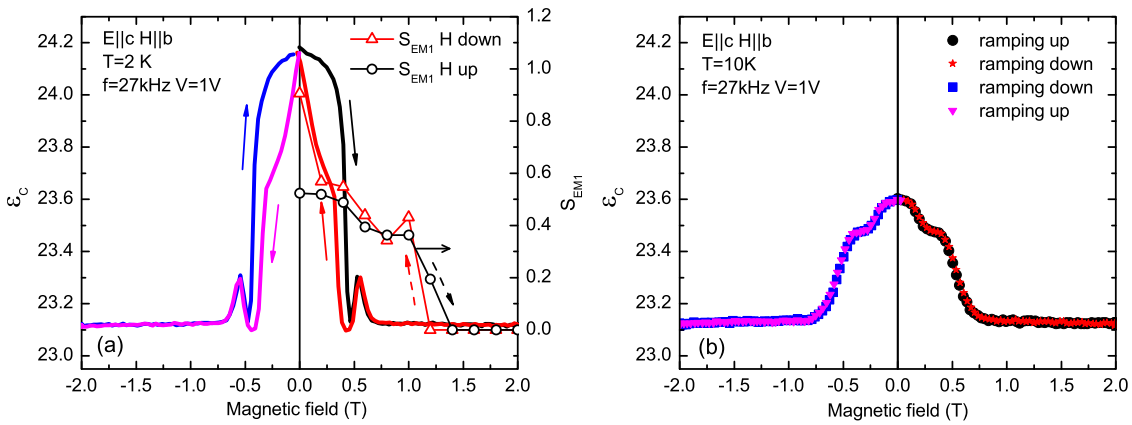

FIG. 10. Magnetic-field ($H \parallel b$) dependence of electric permittivity ε_c of a $DyFeO_3$ single crystal measured at (a) $T = 2$ K and (b) 10 K, i.e., below and above $T_N^{Dy} = 4.2$ K. The red curve with the open triangles and the black curve with the open circles in (a) show contribution of the electromagon EM_1 to the static ε. No hysteresis in $\varepsilon(H)$ was observed at $T = 10$ K.

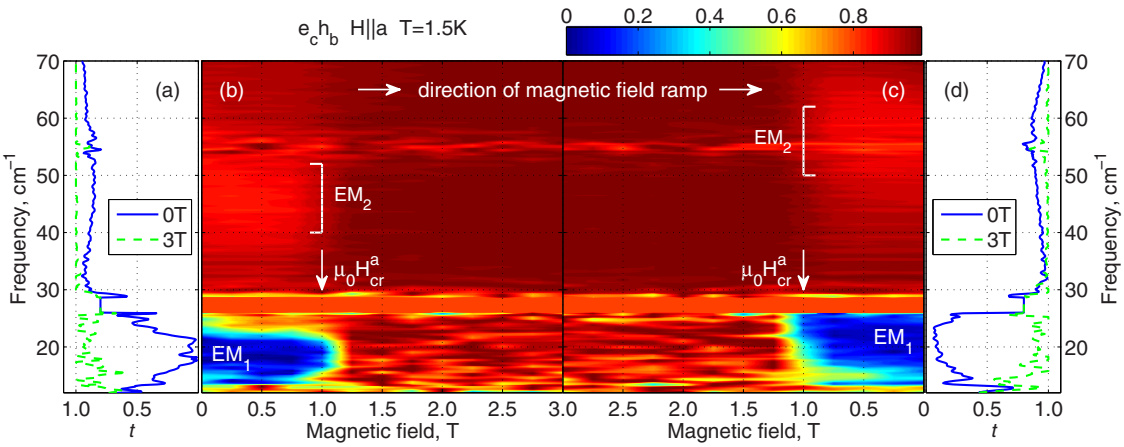

FIG. 11. Magnetic-field ($H \parallel a$) dependence of normalized transmittance t measured in the $e_c h_b$ configuration at $T = 1.5$ K during ramping field (a) and (b) up and (c) and (d) down. (a) Two spectra for normalized transmittance t measured at $\mu_0 H = 0$ T($H < H^a_{cr}$) and 3 T ($H > H^a_{cr}$) during ramping field up. (b) A normalized transmittance map vs magnetic field and light frequency measured during ramping field up. (c) A normalized transmittance map measured during ramping field down. (d) Two spectra for normalized transmittance t measured at $\mu_0 H = 0$ T ($H < H^a_{cr}$) and 3 T ($H > H^a_{cr}$) during ramping field down. An artifact of the measurement between 27 and 29 cm^{-1} is smeared out in the color map. Critical magnetic field $\mu_0 H^a_{cr} \approx 1$ T in (b) and (c) is shown with vertical arrows.

down (c) and (d). With increasing the field starting from $H_a = 0$ the EM_1 and EM_2 electromagnons at 18 and 48 cm^{-1} are observed up to $\mu_0 H^a_{cr} \approx 1$ T and vanish at $H > H^a_{cr}$. With decreasing the magnetic field at $H < H^a_{cr}$ the $EM_{1,2}$ appear again but in slightly different positions: EM_1 appears at 20 cm^{-1}, and EM_2 appears at 57 cm^{-1}. We note here that a weak shift in the EM_1 and EM_2 lines was also observed in the temperature dependence of transmission spectra in the $e_c h_b$ configuration in zero magnetic field (see Fig. 4): with the temperature increase from 2 to 4 K, the EM_1 line changes its position from 20 to 22 cm^{-1}, and the EM_2 line shifts from 48 to 55 cm^{-1}.

IV. DISCUSSION AND CONCLUSIONS

A. Quasi-FM mode hardening below T_N^{Dy}

Figure 1 shows that the frequency of the quasi-FM mode increases from 14 to 19 cm^{-1} below $T_N^{Dy} = 4.2$ K when the ordering of Dy spins occurs in the ab plane. The observed magnon hardening indicates a strong Dy-Fe interaction. Below T_N^{Dy}, only the lowest $|\pm 15/2\rangle$ Dy doublet is populated, and thus, it governs the magnetic properties of Dy subsystem at these temperatures. For our estimations we will consider the Dy subsystem in a two sublattice approximation with the Dy moments ordered in a collinear antiferromagnetic structure in the ab plane. In this case, the magnetization M_{Dy} of one of the two Dy sublattices below $T_N^{Dy} = 4.2$ K can be described in the Weiss mean-field theory approach as follows:

$$M_{Dy}(H_{eff}) = N\mu_{Dy} \tanh\left(\frac{\mu_{Dy}\lambda M_{Dy}}{k_B T}\right). \quad (1)$$

Here N is a number of Dy^{3+} ions in one of the sublattices per unit volume; μ_{Dy} is a magnetic moment of a split Dy ground state doublet sublevel $\mu_{Dy} \approx 9.2\mu_B$ [3,33]; $\tanh(x)$ is a Brillouin function $B_S(x)$ for $S = 1/2$ (since only the lowest Dy doublet level is relevant); λ is a mean-field constant. Introducing reduced magnetization $m = M_{Dy}/N\mu_{Dy}$ and reduced temperature $t = Tk_B/N\mu^2_{Dy}\lambda$ Eq. (1) can be rewritten as

$$m = \tanh(x), \quad m = xt. \quad (2)$$

Solving graphically Eqs. (2) we obtain reduced magnetization at a given reduced temperature, where $m = 1$ corresponds to the saturated magnetization $M_{Dy} = N\mu_{Dy}$ and $t = 1$ corresponds to the Néel temperature $T_N^{Dy} = N\mu^2_{Dy}\lambda/k_B$. The obtained temperature dependence of M_{Dy} is shown in the inset of Fig. 1 in normalized units with the black solid curve. The quasi-FM mode frequency below T_N^{Dy} can be described as follows:

$$\omega_{FM}(T) = 14\,\text{cm}^{-1} + kM_{Dy}(T), \quad (3)$$

where k is a matching coefficient. Using Eq. (3) we demonstrate that the calculated frequency $\omega_{FM}(T)$ nicely correlates with the experimental data below T_N^{Dy} (see the inset of Fig. 1).

B. Effective g-factor of the quasi-FM mode at $T < T_N^{Dy}$

Figure 6 shows that at $T = 1.5$ K and $H > H^c_{cr}$ when Fe spins are in the $\Gamma_4(G_x F_z)$ phase, the frequency of the quasi-FM mode linearly depends on the external magnetic field along the c axis with effective g-factor $g_{eff} \approx 2.1$. The frequency of the quasi-FM mode can be obtained from the equations of motion of magnetic order parameters G and F,

$$\frac{d\vec{F}}{dt} = -\gamma[\vec{F} \times \vec{H}_F] - \gamma[\vec{G} \times \vec{H}_G],$$
$$\frac{d\vec{G}}{dt} = -\gamma[\vec{F} \times \vec{H}_G] - \gamma[\vec{G} \times \vec{H}_F], \quad (4)$$

where $\vec{G} = (\vec{M}_1 - \vec{M}_2)/2$, $\vec{F} = (\vec{M}_1 + \vec{M}_2)/2$ are antiferro- and ferromagnetism vectors, $\vec{M}_{1,2}$ are magnetic moments of Fe sublattices, $\vec{H}_F = -\partial\Phi/\partial\vec{F}$, $\vec{H}_G = -\partial\Phi/\partial\vec{G}$, $\gamma \approx 2\mu_B/\hbar$ is the gyromagnetic ratio for Fe spins and Φ is the nonequilibrium

thermodynamic potential of $DyFeO_3$. At low temperatures when only the lowest Dy doublet is populated and the Dy subsystem is paramagnetic Φ is given by the expression [36],

$$\Phi = 1/2A\vec{F}^2 + 1/2\tilde{b}_2 G_y^2 + 1/2\tilde{b}_3 G_z^2 + d_1 G_x F_z + d_3 G_z F_x - (1+\eta_z) F_z H_z - \tau_1 G_x H_z + \text{fourth-order terms}, \quad (5)$$

where A and $d_1 \approx -d_3 = -d$ are isotropic and antisymmetric Dzyaloshinskii-Morija constants; $\tilde{b}_2$ and $\tilde{b}_3$ are anisotropy constants renormalized by Dy-Fe interaction; $\eta_z = \chi_c \lambda_F$ and $\tau_1 \approx \chi_c \lambda_G \cos\varphi_0$, where χ_c is a Van Vleck susceptibility of Dy ions along the c axis, λ_F and λ_G are constants of the isotropic and anisotropic Dy-Fe exchange interactions. Linearizing and solving Eqs. (4) using the thermodynamic potential Φ from Eq. (5) the following expression for ω_{FM} ($H \parallel c$) can be obtained for the $\Gamma_4(G_x F_z)$ phase of Fe spins: $\omega_{FM} = \sqrt{\omega_0^2 + \gamma^2 H(H + H_D^{eff})}$, where ω_0 is the magnon's frequency in zero field, and H_D^{eff} is the effective Dzyaloshinskii field. In external magnetic fields which are small compared to H_D^{eff} the frequency ω_{FM} can be written as follows:

$$\omega_{FM} \approx \omega_0 + \frac{\gamma^2 H_D^{eff}}{2\omega_0} H. \quad (6)$$

We note that Eq. (6) was derived using thermodynamic potential (5) where the Dy subsystem was considered paramagnetic. For more accurate results at $T < T_N^{Dy}$, weak interaction between Dy magnetic moments should be taken into account in the expression for thermodynamic potential Φ. At the same time as a first approximation we will use Eq. (6) to estimate the Dzyaloshinskii field H_D^{eff} at $T < T_N^{Dy}$. At $T = 1.5$ K ω_{FM} linearly depends on the external magnetic field along the c axis $\omega_{FM} = \omega_{FM}^{extrap} + g_{eff}\mu_B\mu_0 H$ where $g_{eff} \approx 2.1$ and $\omega_0 = \omega_{FM}^{extrap} \approx 15.2\,cm^{-1}$ [see Fig. 6(b)]. Comparing this to Eq. (6) we get $\mu_0 H_D^{eff} \approx 34$ T. Earlier room-temperature studies of quasi-FM mode behavior in the magnetic field $H \parallel c$ showed that $\mu_0 H_D^{eff}$ in $DyFeO_3$ is 16.5 T [31] which is smaller by a factor of ~2 compared to the value we obtained for $T = 1.5$ K. Taking into account that Dzyaloshinskii field H_D practically does not depend on temperature in $YFeO_3$ [41,42] where Y is a nonmagnetic ion, the increase in H_D^{eff} at low temperatures in $DyFeO_3$ can be attributed to the increase in the Dy-Fe interaction.

C. Contribution of the electromagnon EM_1 to the static ε upon cycling of magnetic field $H \parallel b$ at $T < T_N^{Dy}$

To evaluate the contribution of the electromagnon excitation EM_1 to the changes in $\varepsilon_c(H)$ shown in Fig. 10(a) the transmission spectra from Fig. 9 were modeled and fitted. The obtained magnetic-field-dependent parameters of the EM_1 excitation, such as oscillator strength S_{EM}, eigenfrequency ω_{EM}, and damping constant γ_{EM} are shown in Table II. The modeling of transmission spectra measured during ramping the field up was more complicated and less reliable as the form of the EM_1 spectral line was not nicely fitted with one oscillator and required introduction of two closely positioned and overlapping Lorentz oscillators. For this reason in Table II we indicate only the combined oscillator strength of two

TABLE II. Parameters of the EM_1 electromagnon [see Eq. (7)] obtained from the modeling of the transmission spectra of $DyFeO_3$ measured in the $e_c h_a$ configuration at $T = 1.5$ K as the magnetic field was ramped up from 0 to 2 T and then down from 2 T to 0.

$\mu_0 H$ (T)	S_{EM1}^{up}	S_{EM1}^{down}	ω_{EM1}^{down} (cm^{-1})	γ_{EM1}^{down} (cm^{-1})
2–1.4	0	0		
1.2	0.19	0		
1.0	0.36	0.43	29.8	33
0.8	0.36	0.34	29.8	30
0.6	0.39	0.44	29.4	14
0.4	0.49	0.55	30.2	15
0.2	0.52	0.57	28.5	13.4
0	0.52	0.9	17.5	9.3

Lorentz oscillators used for the fit of EM_1 during ramping the field up and do not indicate the eigenfrequency and damping constant of EM_1. The contribution to the electric susceptibility spectrum due to the EM_1 excitation can be described using a Lorentz oscillator,

$$\chi_{EM}(\omega) = \frac{S_{EM}\omega_{EM}^2}{\omega_{EM}^2 - \omega^2 + i\gamma_{EM}\omega}. \quad (7)$$

At $\omega = 0$ Eq. (7) gives the EM_1 contribution to static permittivity ε_c: $\Delta\varepsilon_{EM} = \chi_{EM}(0) = S_{EM}$ which is equal to the oscillator strength of the EM_1 excitation. The magnetic-field dependence of S_{EM} from Table II is plotted in Fig. 10(a) above the high-field value of $\varepsilon_c \approx 23.1$ (black curve with open circles for ramping field up and red curve with open triangles for ramping field down). At low magnetic fields ($H < H_{cr}^b$) $S_{EM} \sim 0.5$ and accounts for ~45% of the total change of quasistatic ε_c during the cycling of magnetic field [$\Delta\varepsilon_{max}(1.5\,K) = 24.2 - 23.1 = 1.1$]. Figure 10(b) shows the $\varepsilon_c(H)$ hysteresis loop measured at $T = 10$ K that is above T_N^{Dy}. At this temperature $\varepsilon_c(H)$ does not manifest any hysteresis. At the same time ε_c still experiences change $\Delta\varepsilon_{max}(10K) \approx 0.6$ during the spin-reorientation transition of the Fe subsystem at $\mu_0 H_{cr}^b = 0.6$ T, which is no longer related to the contribution from the electromagnon EM_1. The difference between the total change in quasistatic ε_c observed during the cycling of the magnetic field at $T = 1.5$ and 10 K is $\Delta\varepsilon_{max}(1.5K) - \Delta\varepsilon_{max}(10K) = 0.5$ which is close to the oscillator strength of EM_1 in low magnetic fields ($S_{EM} \sim 0.5$) indicating that this difference can be mainly due to the contribution from the electromagnon EM_1.

V. CONCLUSIONS

We have studied magnetic excitations in a $DyFeO_3$ single crystal in the far-IR spectral region in external magnetic fields along all three main crystallographic directions and low temperatures down to 1.5 K, i.e., below T_N^{Dy}. The frequencies of both quasi-FM and quasi-AFM magnon modes demonstrate hardening upon magnetic ordering of Dy spins at $T_N^{Dy} = 4.2$ K that can be attributed to the appearance of an additional effective magnetic field at Fe sites due to Dy-Fe interaction. The quasi-FM mode's g-factor along the c axis at $T < T_N^{Dy}$ and low external magnetic fields is zero; at high enough magnetic

fields when the Fe subsystem is at the Γ_4 spin configuration $g_{\text{eff}} = 2.1$ which is nearly twice as big as reported earlier for $T = 300\,\text{K}$. The increase in g_{eff} can be attributed to the renormalization of the effective Dzyaloshinskii field H_D^{eff} due to the increase in Dy-Fe interaction at low temperatures. Two electric dipole-active magnetic excitations EM_1 and EM_2, or electromagnons, have been found at ~ 20 and $\sim 50\,\text{cm}^{-1}$ in the magnetoelectric phase of $DyFeO_3$ below T_N^{Dy}. The electromagnons vanish with the application of a strong enough magnetic field along the a or b axis which changes the magnetic structures of the Fe^{3+} and Dy^{3+} moments into the ones compatible with spatial inversion symmetry. We show that the electromagnon at $\sim 20\,\text{cm}^{-1}$ provides a significant contribution to the static electric permittivity ε. The energies of the electromagnons as well as static electric permittivity manifest a strong hysteresis upon cycling of the external magnetic field at $T < T_N^{\text{Dy}}$.

ACKNOWLEDGMENTS

The authors are grateful to R. Basistyy for help with modeling of experimental data and to S. Artyukhin for interest and useful discussions. Work at the New Jersey Institute of Technology and Rutgers University was supported by the U.S. Department of Energy under Contract No. DE-FG02-07ER46382. Use of the National Synchrotron Light Source, Brookhaven National Laboratory, was supported by the U.S. Department of Energy under Contract No. DE-AC02-98CH10886.

[1] M. Marezio, J. P. Remeika, and P. D. Dernier, The Crystal Chemistry of Rare Earth Orthoferrites, Acta Crystallogr., Sect. B: Struct. Crystallogr. Cryst. Chem. **26**, 2008 (1970).

[2] R. L. White, Review of Recent Work on the Magnetic and Spectroscopic Properties of the Rare-Earth Orthoferrites, J. Appl. Phys. **40**, 1061 (1969).

[3] G. Gorodetsky, B. Sharon, and S. Shtrikman, Magnetic Properties of an Antiferromagnetic Orthoferrite, J. Appl. Phys. **39**, 1371 (1968).

[4] K. P. Belov, A. K. Zvezdin, A. M. Kadomtseva, and I. B. Krynetskii, New orientational transitions induced in orthoferrites by an external field, Sov. Phys. JETP **40**, 980 (1975).

[5] A. Berton and B. Sharon, Specific Heat of $DyFeO_3$ from 1.2°–80 ° K, J. Appl. Phys. **39**, 1367 (1968).

[6] C. E. Johnson, L. A. Prelorendjo, and M. F. Thomas, Field induced spin reorientation in orthoferrites $DyFeO_3$, $HoFeO_3$ and $ErFeO_3$, J. Magn. Magn. Mater. **15**, 557 (1980).

[7] T. Yamaguchi and K. Tsushima, Magnetic Symmetry of Rare-Earth Orthochromites and Orthoferrites, Phys. Rev. B **8**, 5187 (1973).

[8] Y. Tokunaga, S. Iguchi, T. Arima, and Y. Tokura, Magnetic-Field-Induced Ferroelectric State in $DyFeO_3$, Phys. Rev. Lett. **101**, 097205 (2008).

[9] N. Kida and Y. Tokura, Terahertz magnetoelectric response via electromagnons in magnetic oxides, J. Magn. Magn. Mater. **324**, 3512 (2012).

[10] A. P. Pyatakov and A. K. Zvezdin, Magnetoelectric and multiferroic media, Phys.-Usp. **55**, 557 (2012).

[11] V. N. Krivoruchko, Electrically active magnetic excitations in antiferromagnets (Review Article), Low Temp. Phys. **38**, 807 (2012).

[12] A. Pimenov, A. M. Shuvaev, A. A. Mukhin, and A. Loidl, Electromagnons in multiferroic manganites, J. Phys.: Condens. Matter **20**, 434209 (2008).

[13] D. Senff, N. Aliouane, D. N. Argyriou, A. Hiess, L. P. Regnault, P. Link, K. Hradil, Y. Sidis, and M. Braden, Magnetic excitations in a cycloidal magnet: the magnon spectrum of multiferroic $TbMnO_3$, J. Phys.: Condens. Matter **20**, 434212 (2008).

[14] N. Kida, Y. Takahashi, J. S. Lee, R. Shimano, Y. Yamasaki, Y. Kaneko, S. Miyahara, N. Furukawa, T. Arima, and Y. Tokura, Terahertz time-domain spectroscopy of electromagnons in multiferroic perovskite manganites, J. Opt. Soc. Am. B **26**, A35 (2009).

[15] A. Pimenov, A. Shuvaev, A. Loidl, F. Schrettle, A. A. Mukhin, V. D. Travkin, V. Y. Ivanov, and A. M. Balbashov, Magnetic and Magnetoelectric Excitations in $TbMnO_3$, Phys. Rev. Lett. **102**, 107203 (2009).

[16] A. M. Shuvaev, V. D. Travkin, V. Y. Ivanov, A. A. Mukhin, and A. Pimenov, Evidence of Electroactive Excitation of The Spin Cycloid in $TbMnO_3$, Phys. Rev. Lett. **104**, 097202 (2010).

[17] S. Pailhès, X. Fabrèges, L. P. Régnault, L. Pinsard-Godart, I. Mirebeasu, F. Moussa, M. Hennion, and S. Petit, Hybrid Goldstone modes in multiferroic $YMnO_3$ studied by polarized inelastic neutron scattering, Phys. Rev. B **79**, 134409 (2009).

[18] A. B. Sushkov, R. Valdés Aguilar, S. Park, S.-W. Cheong, and H. D. Drew, Electromagnons in Multiferroic YMn_2O_5 and $TbMn_2O_5$, Phys. Rev. Lett. **98**, 027202 (2007).

[19] I. Kézsmárki, N. Kida, H. Murakawa, S. Bordács, Y. Onose, and Y. Tokura, Enhanced Directional Dichroism of Terahertz Light in Resonance with Magnetic Excitations of the Multiferroic $Ba_2CoGe_2O_7$ Oxide Compound, Phys. Rev. Lett. **106**, 057403 (2011).

[20] S. P. P. Jones, S. M. Gaw, K. I. Doig, D. Prabhakaran, E. M. Hétroy Wheeler, A. T. Boothroyd, and J. Lloyd-Hughes, High-temperature electromagnons in the magnetically induced multiferroic cupric oxide driven by intersublattice exchange, Nat. Commun. **5**, 3787 (2014).

[21] M. Cazayous, Y. Gallais, A. Sacuto, R. de Sousa, D. Lebeugle, and D. Colson, Possible Observation of Cycloidal Electromagnons in $BiFeO_3$, Phys. Rev. Lett. **101**, 037601 (2008).

[22] P. Rovillain, R. de Sousa, Y. Gallais, A. Sacuto, M. A. Méasson, D. Colson, A. Forget, M. Bibes, A. Barthélémy, and M. Cazayous, Electric-field control of spin waves at room temperature in multiferroic $BiFeO_3$, Nature Mater. **9**, 975 (2010).

[23] A. M. Kuzmenko, A. Shuvaev, V. Dziom, A. Pimenova, M. Schiebl, A. A. Mukhin, V. Y. Ivanov, L. N. Bezmaternykh, and A. Pimenov, Giant gigahertz optical activity in multiferroic ferroborate, Phys. Rev. B **89**, 174407 (2014).

[24] N. Kida, D. Okuyama, S. Ishiwata, Y. Taguchi, R. Shimano, K. Iwasa, T. Arima, and Y. Tokura, Electric-dipole-active magnetic resonance in the conical-spin magnet $Ba_2Mg_2Fe_{12}O_{22}$, Phys. Rev. B **80**, 220406(R) (2009).

[25] N. Kida, S. Kumakura, S. Ishiwata, Y. Taguchi, and Y. Tokura, Gigantic terahertz magnetochromism via electromagnons in the hexaferrite magnet $Ba_2Mg_2Fe_{12}O_{22}$, Phys. Rev. B **83**, 064422 (2011).

[26] S. Seki, N. Kida, S. Kumakura, R. Shimano, and Y. Tokura, Electromagnons in the Spin Collinear State of a Triangular Lattice Antiferromagnet, Phys. Rev. Lett. **105**, 097207 (2010).

[27] R. M. White, R. J. Nemanich, and Conyers Herring, Light scattering from magnetic excitations in orthoferrites, Phys. Rev. B **25**, 1822 (1982).

[28] S. Venugopalan, M. Dutta, A. K. Ramdas, and J. P. Remeika, Magnetic and vibrational excitations in rare-earth orthoferrites: A Raman scattering study, Phys. Rev. B **31**, 1490 (1985).

[29] A. M. Balbashov, A. A. Volkov, S. P. Lebedev, A. A. Mukhin, and A. S. Prokhorov, High-frequency magnetic properties of dysprosium orthoferrite, Sov. Phys. JETP **61**, 573 (1985).

[30] S. M. Shapiro, J. D. Axe, and J. P. Remeika, Neutron-scattering studies of spin waves in rare-earth orthoferrites, Phys. Rev. B **10**, 2014 (1974).

[31] A. M. Balbashov, G. V. Kozlov, A. A. Mukhin, and A. S. Prokhorov, Submillimeter spectroscopy of antiferromagnetic dielectrics: rare-earth orthoferrites, in *High Frequency Processes in Magnetic Materials*, edited by G. Srinivasan, A. Slavin (World Scientific, Singapore, 1995), Part I, pp. 56–98.

[32] V. G. Bar'yakhtar, I. M. Vitebskii, and D. A. Yablonskii, Symmetry and magnetic-resonance frequencies in magnetically ordered crystals, Sov. Phys. JETP **49**, 703 (1979).

[33] H. Schuchert, S. Hofner, and R. Faulhaber, Optical Investigation of $DyFeO_3$, Z. Phys. **220**, 273 (1969).

[34] I. Nowik and H. J. Williams, Magnetic properties and paramagnetic relaxation of dysprosium in $DyFeO_3$ below the Curie point, Phys. Lett. **20**, 154 (1966).

[35] K. P. Belov, A. K. Zvezdin, A. M. Kadomtseva, and I. B. Krynetskii, New orientational transitions induced in orthoferrites by an external field, Sov. Phys. JETP **40**, 980 (1974).

[36] A. K. Zvezdin and V. M. Matveev, Theory of the magnetic properties of dysprosium orthoferrite, Sov. Phys. JETP **50**, 543 (1979).

[37] S. L. Gnatchenko, K. Piotrowski, A. Szewczyk, R. Szymczak, and H. Szymczak, Two-step metamagnetic phase transition induced by a magnetic field parallel to the b-axis in $DyFeO_3$, J. Magn. Magn. Mater. **129**, 307 (1994).

[38] S. L. Gnatchenko, N. F. Kharchenko, P. P. Lebedev, K. Piotrowski, H. Szymczak, and R. Szymczak, Magneto-optical studies of H-T phase diagram for $DyFeO_3$ ($H \parallel a$), J. Magn. Magn. Mater. **81**, 125 (1989).

[39] D. A. Yablonskii and V. N. Krivoruchko, Antiferroelectric resonance in rare-earth orthoferrites, Sov. Phys. Solid State **30**, 1765 (1988).

[40] Z. Y. Zhao, X. Zhao, H. D. Zhou, F. B. Zhang, Q. J. Li, C. Fan, X. F. Sun, and X. G. Li, Ground state and magnetic phase transitions of orthoferrite $DyFeO_3$, Phys. Rev. B **89**, 224405 (2014).

[41] A. M. Balbashov, A. G. Berezin, Y. M. Gufan, G. S. Kolyadko, P. Y. Marchukov, and E. G. Rudashevskii, Soft mode and energy gap in spin-wave spectrum in a second-order orientational phase transition. AFMR in $YFeO_3$, Sov. Phys. JETP **66**, 174 (1987).

[42] S. Jacobs, H. F. Burne, and L. M. Levinson, Field-Induced Spin Reorientation in $YFeO_3$ and $YCrO_3$, J. Appl. Phys. **42**, 1631 (1971).